

Reconstruction of major fibers using 7T multi-shell Hybrid Diffusion Imaging in mice

Madelaine Daianu^{*a,b}, Russell E. Jacobs^c, Berislav V. Zlokovic^d,
Axel Montagne^d, Paul M. Thompson^{a,b}

^aImaging Genetics Center, Mark & Mary Stevens Institute for Neuroimaging & Informatics,
University of Southern California, Marina del Rey, CA, USA

^bDepartment of Neurology, UCLA School of Medicine, Los Angeles, CA, USA

^cBiological Imaging Center, California Institute of Technology, CA, USA

^dZilkha Neurogenetic Institute, Keck School of Medicine, University of Southern California,
CA, USA

ABSTRACT

Diffusion weighted imaging (DWI) can reveal the orientation of the underlying fiber populations in the brain. High angular resolution diffusion imaging (HARDI) is increasingly used to better resolve the orientation and mixing of fibers. Here, we assessed the added value of multi-shell q -space sampling on the reconstruction of major fibers using mathematical frameworks from q -ball imaging (QBI) and generalized q -sampling imaging (GQI), as compared to diffusion tensor imaging (DTI). We scanned a healthy mouse brain using 7-Tesla 5-shell HARDI ($b=1000, 3000, 4000, 8000, 12000$ s/mm²), also known as hybrid diffusion imaging (HYDI). We found that QBI may provide greater reconstruction accuracy for major fibers, which improves with the addition of higher b -value shells, unlike GQI or DTI (as expected). Although QBI is a special case of GQI, the major fiber orientation in QBI was more closely related to the orientation in DTI, rather than GQI. HYDI can aid the clinical outcomes of research and especially – more advanced human and animal connectomics projects to map the brain's neural pathways and networks.

Keywords: DWI, multi-shell, HARDI, HYDI, mouse, QBI

1. INTRODUCTION

Diffusion-weighted imaging (DWI) is a powerful and widely used tool to study water diffusion in the brain. DWI has revolutionized our understanding of the brain's "connectome" – revealing the complex network architecture of the living brain and its fiber connections [1] [2] [3].

DWI can reveal the architecture and orientation of the neural tissue by sampling the diffusion of water at multiple spherical angles [4] [5] [6]. In this study, we first estimated the directions of the underlying axonal fibers using standard diffusion tensor image (DTI) reconstruction as described by Jiang and colleagues [7]. The DTI model is known to fail to resolve complex structures, especially where fibers mix and cross [8] [5], so we also employed two complex reconstruction frameworks – q -ball imaging (QBI) and generalized q -sampling imaging (GQI), to overcome limitations of DTI. QBI and GQI frameworks used here are model-free q -space imaging methods that describe the Fourier transform relationship between the diffusion MR signal and the distribution of spins undergoing diffusion within individual voxels [5]. For QBI and GQI, we computed the orientation distribution function (ODF) of the diffusion displacement and evaluated their performance in resolving major fibers in a shell-sampling scheme. These were also compared to the reconstruction of the major fibers from DTI.

We tested out these mathematical reconstruction frameworks – DTI, QBI and GQI, on 5-shell HARDI data (300 diffusion gradients; 60 per shell), also known as *hybrid* diffusion imaging (HYDI), acquired in a healthy mouse model. Although HYDI was previously studied in humans, this may be the first acquisition of HYDI in mouse brain, where voxel sizes are more than 1000 times smaller than in conventional human DWI scans and longer scan times can resolve very fine tissue structure [4]. Here we show that among the three distinct reconstruction methods, QBI may offer the most accurate reconstruction for the major fibers while taking advantage of the multi-shell sampling scheme to reduce the angular reconstruction error. These findings are not only important for the imaging research community, but also for those who seek to validate DWI parameters versus histological correlates in experimental mouse models of disease.

*madelaine.daianu@ini.usc.edu

2. METHODS

2.1 Data Acquisition and Processing

We scanned one wild-type mouse *ex vivo* with a 7 Tesla Bruker BioSpin MRI scanner at California Institute of Technology. We used a 3D 8-segment spin echo EPI sequence to acquire the images (120x166x80 matrix; voxel size: 0.1x0.1x0.2 mm³, TE=34 ms; TR=500 ms, $\delta=11$ ms, $\Delta=16$ ms), yielding a 20-hour scan time. 60 diffusion-weighted volumes and 5 T2-weighted volumes with no diffusion sensitization (b_0 image) were acquired. DWIs were acquired with the same angular sampling at 5 b -values: 1000, 3000, 4000, 8000 and 12000 s/mm². During preprocessing, we corrected for eddy current distortions using the “eddy correct FSL” tool (www.fmrib.ox.ac.uk/fsl) for which a corrected gradient table was calculated to account for the distortions. Extra-cerebral tissue was removed using the “skull-stripping” Brain Extraction Tool from BrainSuite (<http://brainsuite.org/>). All images were linearly aligned and up-sampled to the DWI Mori template (at voxel size: 0.065x0.065x0.065 mm³) (<http://cmrm.med.jhmi.edu/>) using FSL’s *flirt* function with 12 degrees of freedom; the gradient direction table was rotated accordingly.

2.2 Image Reconstruction and Tractography

First, we reconstructed the tensors within every voxel for single-shell DWIs and multi-shell HYDIs using DTI-based reconstruction as implemented in DTI Studio [7] and currently in DSI Studio (www.dsi-studio.labsolver.org). Next, we used QBI [6] [8] [9] and GQI [5] based on spherical harmonics transformations [8]; QBI and GQI can resolve complex intravoxel white matter structure, unlike DTI, and were used here to compute the diffusion orientation distribution function (dODF) in each voxel and the spin distribution function (SDF), which is a normalized dODF used in GQI (detailed below). Both QBI and GQI used the Funk-Radon transform to reconstruct the images; QBI is a special case of GQI with a finite diffusion sampling length [5].

K -space and q -space imaging methods rely on the Fourier transform to define the relationship between the diffusion MR signal, $S(k,q)$, average diffusion propagator, $p_\Delta(r,R)$ for time Δ , and the diffusion spin density, $p_\Delta(r)$ [5] [6]. From the k -space reconstruction, the diffusion weighted image can be derived, $W(r,q)$, as a function of the average propagator at each voxel:

$$W(r,q) = \int \rho(r)p_\Delta(r,R)e^{i2\pi q \cdot R} dR \quad (1)$$

where r is the voxel coordinate, $q = \gamma G \delta / 2\pi$ where γ is the gyromagnetic ratio, and G and δ are the strength and duration of the encoding gradient; finally, R is the diffusion displacement [5]. In Eq. 1, $\rho(r)p_\Delta(r,R)$ represents the spin density function, or $Q(r,R)$, and defines the diffusion average propagator in the scale of the spin quantity. By applying the cosine transform to Eq. 1, $Q(r,R)$ can be redefined as:

$$Q(r,R) = \int W(r,q) \cos(2\pi q \cdot R) dq \quad (2)$$

From here, we can quantify the distribution of spins undergoing diffusion in a particular direction \hat{u} :

$$\psi_\rho(r,\hat{u}) = \int_0^{L_\Delta} Q(r,L\hat{u}) dL \quad (3)$$

where L_Δ is the diffusion sampling length, also known as the regularization parameter [6]. Eq. 3 represents the spin distribution function (SDF) and when obtained from the spin density function, $Q(r,R)$, it defines the ODF of the spin quantity. Furthermore, Eqs. 2 and 3 relate the diffusion weighted image, $W(r,q)$, to the SDF [5]:

$$\psi_\rho(r,\hat{u}) = L_\Delta \int W(r,q) \text{sinc}(2\pi L_\Delta q \cdot \hat{u}) dq \quad (4)$$

If L_Δ is set to infinity, the sinc function in Eq. 4 becomes the delta function, and therefore estimates the Funk-Radon transform used by QBI [8]. Meanwhile, if L_Δ is kept finite it can minimize artifacts in the Fourier transform that can give rise to “spiky” ODFs [6]. A diffusion sampling length of $L_\Delta = 1.1$ was used here, to yield a good reconstruction, as previously recommended [6].

As mentioned already, normalizing the SDF turns it into a diffusion ODF (dODF), ψ_d , which may be viewed as a linear summation of multiple dODFs and a background isotropic dODF [6]. Each dODF component may correspond to a fiber population within each voxel, and these were used here for QBI reconstruction. To reconstruct the ODFs for both QBI and GQI, we used an 8-fold tessellated icosahedron, resulting in 642 sampling directions (ODFs are symmetric around the origin, so 321 directions were used); the ODFs were computed in DSI Studio using a spherical harmonic order of 8 to ensure high angular resolution, and a recommended regularization parameter of 0.006 [5] [6] [9]. Using these we computed a quantitative anisotropy index (QA) to quantify the spin population in a given direction (unlike FA, which is a metric for each voxel) [5]. QA is defined by SDF and dODF at the resolved fiber orientation:

$$QA(\hat{u}) = Z_0 (\psi_q(\hat{u}) - I\psi_q) \quad (5)$$

where Z_0 is an SDF scaling factor, ψ_q is the ODF from QBI or GQI, and $I\psi_q$ computes the isotropic component of the ODF [5].

We ran deterministic tractography in DSI Studio with FA as a threshold criterion to determine where fiber tracts terminate in DTI, and QA as a threshold in QBI and GQI. 35,000 fibers were extracted for single-shell DWIs and multi-shell HYDIs and the fiber orientations were defined based on the primary fiber orientations (or local maxima).

2.3 Data Analysis

First, we delineated an ROI within the cingulum of the mouse brain. The cingulum was studied here due to its homogenous fiber distribution for a fair analysis across all reconstruction methods (especially for DTI, where crossing fibers are not defined).

To compare single-shell vs. multi-shell results, we defined the 5-shell HYDI as the ‘ground truth’ and compared the angular performance of the DTI, QBI and GQI reconstruction methods from single-shell DWIs and <5 multi-shell HYDIs (called *target images*) to the angular performance obtained from the ground truth image (where fibers in the cingulum should have an anterior-to-posterior directionality, *i.e.*, *green* in **Figs. 2** and **4**). To do this, we computed the primary fiber orientation in DTI and the largest local maximum for ODFs in QBI and GQI within each voxel in the cingulum. We determined the average minimum angular difference within the ROI, or the inner angle between the fiber orientations corresponding to the local maxima (or primary fibers), between each target image and the ground truth image for each reconstruction method separately:

$$\theta = \min \left| \cos^{-1} \left| \sum_{\max,1} \hat{u} \cdot \hat{u}_{\max,2} \right| \right| \quad (6)$$

Here, $\hat{u}_{\max,1}$ and $\hat{u}_{\max,2}$ are the local maxima peaks within a voxel in the ground truth and target images.

Finally, to evaluate the performance of each reconstruction method against each of the others, we computed angular differences, as defined above, between DTI vs. QBI, DTI vs. GQI and QBI vs. GQI reconstruction methods for each single-shell DWI, and a combination of multi-shell HYDI schemes.

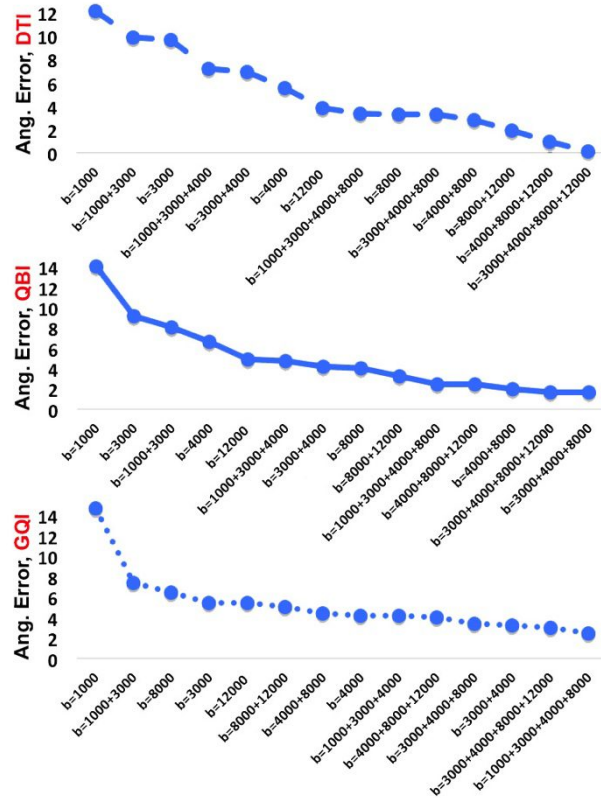


Figure 1. Average angular difference (degrees) in the cingulum between target images and ground truth HYDI reconstructed with DTI, QBI and GQI at single- and multi-shell sampling schemes.

3. RESULTS

3.1 Single- and <5-shell HYDI vs. ground truth HYDI

The largest angular deviation of the primary fiber peaks in the cingulum was 85° in the $b=1000$ s/mm² single shell DTI fiber reconstructions, relative to the ground truth (5-shell HYDI) (**Fig. 1**). This angular difference can occur when the anterior-to-posterior fibers of the cingulum are entirely mistaken for left-to-right fibers (*i.e.*, in the corpus callosum) (**Fig. 2** and **4**). DTI cannot take full advantage of the angular sampling of HYDI data, so we did not expect the DTI reconstructions to improve with the addition of higher b -value shells. We performed a 2-tailed t -test and did not find any significant differences between angular accuracies for the single-shell vs. ≥ 2 -shell reconstructions for DTI.

For QBI, the largest angular deviation of the major peak fibers was 32° ; this angle was also found in the $b=1000$ s/mm² vs. ground truth HYDI comparisons (**Fig. 1**). Unlike DTI, QBI reconstructions across ≥ 2 -shells significantly improved when compared to single-shell reconstructions (had lower angular difference) as indicated by a 2-tailed t -test (p -value = 0.016). We corrected for the three statistical tests performed in this section by setting the p -value threshold to 0.05/3.

The largest angular deviation between the major peaks reconstructed using GQI was 48° for the b -value=1000 s/mm² vs. ground truth HYDI comparisons. Surprisingly, adding shells to the single-shell reconstruction schemes did not significantly reduce the angular difference between single-shell vs. ≥ 2 -shells HYDI reconstructions using GQI.

3.2 Evaluation of DTI, QBI and GQI reconstructions

The angular differences were computed for DTI vs. QBI, DTI vs. GQI and QBI vs. GQI reconstruction methods for all 5-single shells and 9 distinct combinations of ≥ 2 -shells HYDIs as performed in *Section 3.1*.

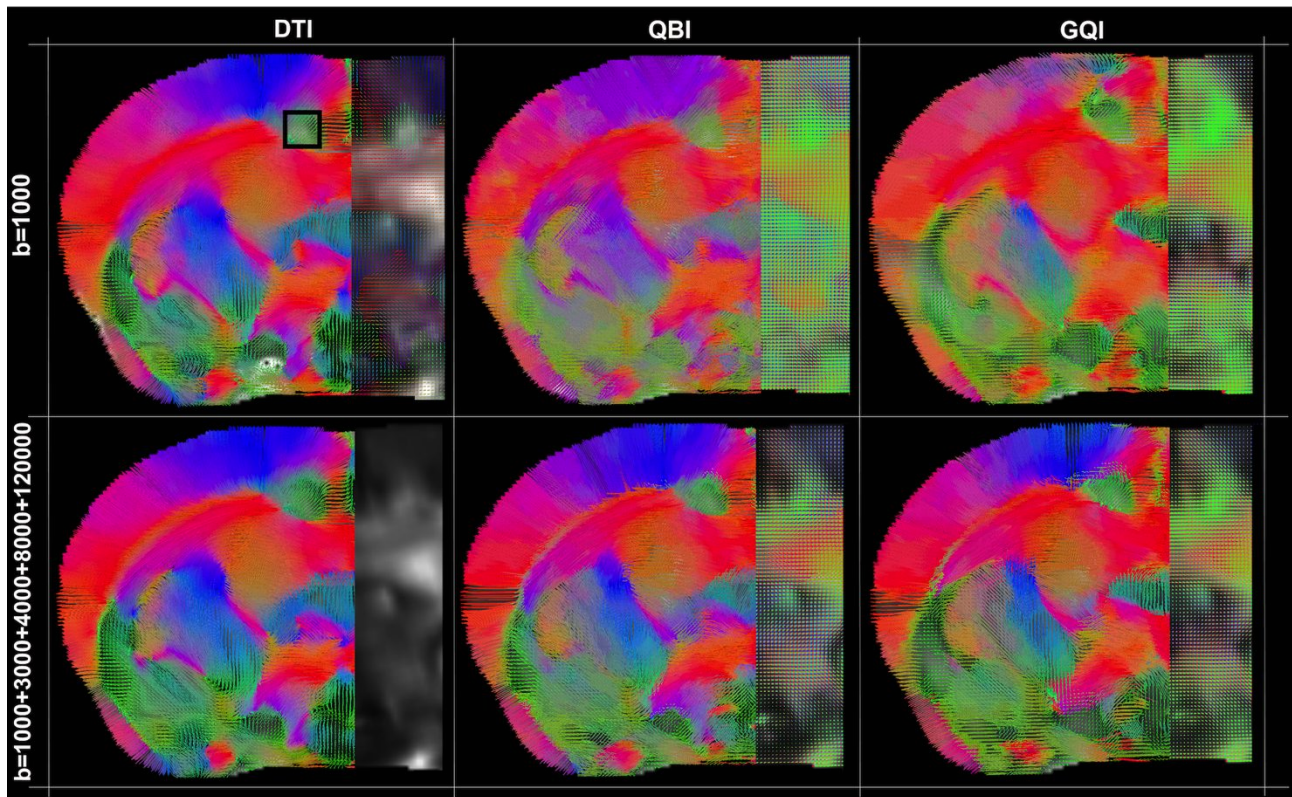


Figure 2. Deterministic streamline fiber tracts from DTI, QBI and GQI at $b=1000$ s/mm² and ground truth HYDI in a coronal slice of the mouse brain. Tracts are overlaid on the primary fiber and FA maps for DTI and the fiber ODF maps for QBI and GQI.

In a 2-tailed t -test, the average angular differences from the DTI vs. QBI comparisons were significantly lower than the angular differences from DTI vs. GQI comparisons in the mouse cingulum (p -value= 3.2×10^{-5}) (**Fig. 3**). These

indicate that although QBI is a special case of GQI – their ability to resolve major fibers is greatly different. Furthermore, the average angular difference in the DTI vs. QBI comparisons was also lower than the angular difference obtained from the QBI vs. GQI comparisons (p -value= 4.8×10^{-3}) (Fig. 3). This further indicates that GQI leads to a larger angular deviation of the major fibers as compared to DTI, as well as QBI – as mentioned above. This also suggests that the resolved major fibers in QBI are closer in their orientation to those resolved through DTI, rather than GQI. As done in the previous section, the p -value threshold was set to 0.05/3 for each of the three statistical tests performed.

Finally, the average angular discrepancy between QBI and GQI was not significantly different from the mean angular difference computed for DTI vs. GQI (Fig. 3). These reinforce our findings above indicating that DTI might infer similar directions for the major fibers to the directions resolved by QBI.

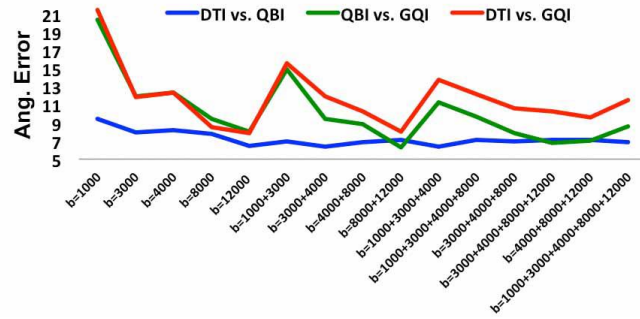


Figure 3. Average angular difference in the mouse cingulum between the different reconstruction methods computed at the same shell-sampling schemes.

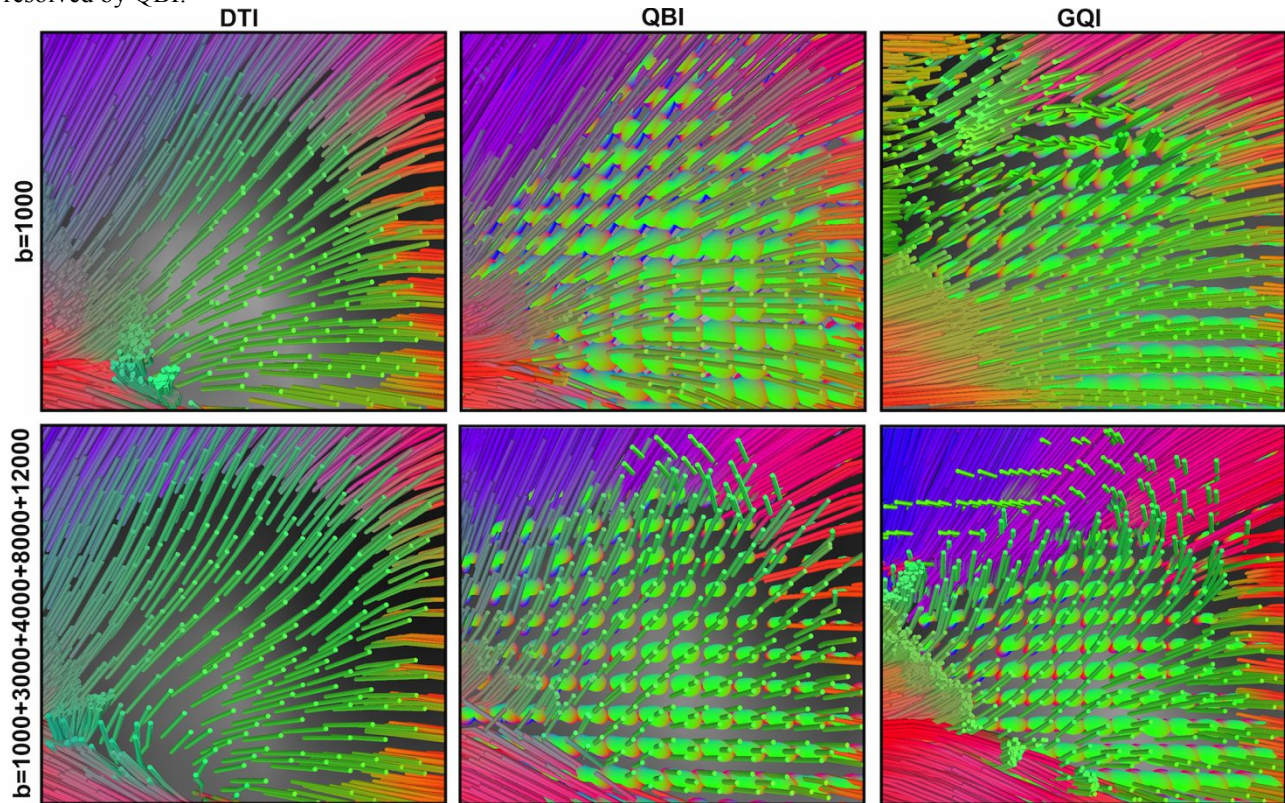


Figure 4. Fiber tracts obtained from deterministic tractography in the mouse cingulum (across a 13x13 voxel area) using DTI, QBI and GQI to reconstruct the fibers from DWIs at b -value=1000 s/mm^2 and ground truth HYDIs. *green fibers = anterior-to-posterior; red fibers= left-to-right; blue fibers=superior-to-inferior.

4. DISCUSSION

In this study we analyzed high-field multi-shell HARDI, or HYDI volumes, from healthy mouse brain to investigate the added value of high b -value shells in reconstructing the major fibers in the cingulum using DTI, QBI and GQI reconstruction frameworks.

QBI and GQI are imaging reconstruction methods that can obtain the orientation of fiber populations from ODFs and SDFs from both single or multi-shell sampling schemes and ODF patterns reconstructed from QBI are thought to be

similar to SDF patterns from GQI [5] [6]. Here, we found that the addition of higher b -value shells to the reconstruction of a multi-shell scheme decreases the angular difference in QBI, but not detectably in GQI (**Figs. 1, 2 and 4**), when compared to reconstructions using 5-shell HYDI. One feasible explanation may be that GQI might perform more accurately if the TE were adjusted for each b -value shell; here, a longer TE was used across all shells, which might possibly allow greater noise in the lower b -value shells. Moreover, in DTI, we did not find any detectable added value of the multi-shell schemes – as expected, however, the reconstructions of the major fibers in QBI were quantitatively more similar to those reconstructed from DTI (**Fig. 3**). The deterministic tractography generated from these is also visually more similar (**Figs. 2 and 4**).

We previously showed that although low b -value shells have a higher signal to noise ratio (SNR) as computed from QA maps in QBI (using deconvoluted dODFs, unlike here), they also lead to a higher angular difference, compared to higher b -value shells [4]. This is in line with our current findings indicating that raw dODFs from QBI might improve when adding higher b -value shells and may be most suitable for assessing HYDI data. These findings will be especially useful in future work when we will compare *ex vivo* HYDI to cellular measures from histological correlates. HYDI may be valuable in human connectome projects [10] [11] [12] [13] [14] [15] and clinical research, as well as magnetic resonance research in experimental animals.

REFERENCES

- [1] A. W. Toga, and P. M. Thompson, "Connectomics sheds new light on Alzheimer's disease," *Biol Psychiatry*, 73(5), 390-2 (2013).
- [2] M. Daianu, N. Jahanshad, T. M. Nir *et al.*, "Rich club analysis in the Alzheimer's disease connectome reveals a relatively undisturbed structural core network," *Hum Brain Mapp*, 36(8), 3087–3103 (2015).
- [3] M. Daianu, N. Jahanshad, T. M. Nir *et al.*, "Breakdown of brain connectivity between normal aging and Alzheimer's disease: a structural k-core network analysis," *Brain Connect*, 3(4), 407-22 (2013).
- [4] M. Daianu, N. Jahanshad, J. E. Villalon-Reina *et al.*, "7T Multi-shell Hybrid Diffusion Imaging (HYDI) for Mapping Brain Connectivity in Mice," *SPIE Proceedings, Medical Imaging 2015: Image Processing*, 9413, 941309-941309 (2015).
- [5] F. C. Yeh, V. J. Wedeen, and W. Y. Tseng, "Generalized q sampling imaging," *IEEE Trans Med Imaging*, 29(9), 1626-1635 (2010).
- [6] F. C. Yeh, V. J. Wedeen, and W. Y. Tseng, "Estimation of fiber orientation and spin density distribution by diffusion deconvolution," *Neuroimage*, 55(3), 1054-62 (2011).
- [7] H. Jiang, P. C. van Zijl, J. Kim *et al.*, "DtiStudio: resource program for diffusion tensor computation and fiber bundle tracking," *Comput Methods Programs Biomed*, 81(2), 106-16 (2006).
- [8] D. S. Tuch, "Q-ball imaging," *Magn Reson Med*, 52(6), 1358-72 (2004).
- [9] M. Descoteaux, E. Angelino, S. Fitzgibbons *et al.*, "Regularized, fast, and robust analytical Q-ball imaging," *Magn Reson Med*, 58(3), 497-510 (2007).
- [10] M. Daianu, N. Jahanshad, E. L. Dennis *et al.*, "Left versus right hemisphere differences in brain connectivity: 4-Tesla HARDI tractography in 569 twins," *Proc IEEE Int Symp Biomed Imaging*, 526 - 529 (2012).
- [11] F. F. Roussotte, M. Daianu, N. Jahanshad *et al.*, "Neuroimaging and genetic risk for Alzheimer's disease and addiction-related degenerative brain disorders," *Brain Imaging Behav*, 8(2), 217-33 (2014).
- [12] M. Daianu, N. Jahanshad, T. M. Nir *et al.*, "Algebraic Connectivity of Brain Networks Shows Patterns of Segregation Leading to Reduced Network Robustness in Alzheimer's Disease," *Med Image Comput Comput Assist Interv (MICCAI) Computational Diffusion MRI: Springer*, 55-64 (2014).
- [13] M. Daianu, A. Mezher, N. Jahanshad *et al.*, "Spectral Graph Theory and Graph Energy Metrics Show Evidence for the Alzheimer's Disease Disconnection Syndrome in APOE-4 Gene Carriers," *International Symposium of Biomedical Imaging*, 458-461 (2015).
- [14] M. Daianu, G. ver Steeg, A. Mezher *et al.*, "Information-Theoretic Clustering of Neuroimaging Metrics Related to Cognitive Decline in the Elderly," *Med Image Comput Comput Assist Interv (MICCAI) Lecture Notes in Computer Science: Springer, In Press*, (2015).
- [15] M. Daianu, M. F. Mendez, V. G. Baboyan *et al.*, "An advanced white matter tract analysis in frontotemporal dementia and early-onset Alzheimer's disease," *Brain Imaging and Behavior, In Press*, (2015).